

Simulation and Experimental Research on Fuel Spray Characteristics of a Self-pressurized Injector

JI Haocheng¹, LIU Rui^{1*}, LI Jing¹, ZHAI Buyun²

1. School of Mechanical and Power Engineering, Nanjing Tech University, Nanjing 211816, P. R. China;

2. Department of Light Aviation Power Project, Jincheng Group Co., Ltd., Nanjing 210002, P. R. China

(Received 7 January 2022; revised 18 February 2022; accepted 23 February 2022)

Abstract: As a miniaturized direct injection (DI) solution, a self-pressurized injector is of great significance for small aviation piston engines, such as spark-ignited two-stroke heavy-fuel engines. The spray characteristics of DI injectors are an important application prerequisite. In this paper, the computational fluid dynamics (CFD) software AVL Fire is employed to study the spray characteristics. Two types of spray models are established based on the Han Sheet model and the KH-RT model, and simulation works are carried out according to two types of spray tests in the literature. The comparison results show that in the constant volume bomb test, the spray patterns obtained by simulation under the two sets of environmental pressures are similar to those in the experiment, and the simulation spray using the KH-RT model can fit the spray contraction of the near nozzle field and the vortex of the far nozzle field better. In the tube test, the spray patterns obtained by simulation under the five sets of flow velocity are similar to those in the experiment, and the simulation spray using the KH-RT model can fit the spray expansion and the vortex of the far nozzle field better. The RP-3 kerosene spray characteristics of the self-pressurized injector are also experimentally studied, and the results demonstrate that due to the higher viscosity of kerosene, the spray shrinks more easily, resulting in a smaller spray cone angle and larger penetration. Therefore, changes in environmental pressure have greater impact on the kerosene spray pattern.

Key words: direct injection; spray characteristics; piston engine; self-pressurized injector

CLC number: V234 **Document code:** A **Article ID:** 1005-1120(2022)01-0066-13

0 Introduction

In recent years, unmanned aerial vehicles (UAVs) have been widely applied because of their high mobility, safety, and low cost, which can perform certain difficult or dangerous tasks^[1-2]. In the UAV propulsion system, due to the high power and energy densities, the internal combustion engine can provide a longer endurance life than the electric motor^[3]. For piston engines, the spark-ignition (SI) engines require lower structural strength, so their weight is light and the power-to-weight ratio is high^[4]. The two-stroke engines theoretically have twice the power output, which means a higher power-to-weight ratio^[5].

The two-stroke engines exhibit a simple structure, low weight, and high power-to-weight ratio^[6]. However, the unique scavenging process causes a scavenging short circuit-loss^[7]. Due to the risk of gasoline fuel in storage, transportation and usage, special applications are more inclined to heavy fuel with a high flash point, low volatility, and high energy density, such as light diesel and aviation kerosene^[8-10]. But this leads to difficulty in cold starting of the engine and a tendency to knock^[11].

The direct injection (DI) technology is widely used to reduce the emissions, improve the power output and reduce the fuel consumption. For two-stroke engines, the fuel short-circuit loss can be reduced by the delayed injection phase, and a well-at-

*Corresponding author, E-mail: address: timliu@njtech.edu.cn.

How to cite this article: JI Haocheng, LIU Rui, LI Jing, et al. Simulation and experimental research on fuel spray characteristics of a self-pressurized injector[J]. Transactions of Nanjing University of Aeronautics and Astronautics, 2022, 39(1):66-78.

<http://dx.doi.org/10.16356/j.1005-1120.2022.01.007>

omized spray improves the cold starting performance and suppresses the knocking tendency^[12].

Numerous studies adopted the gasoline common rail system to investigate the performance and emissions of heavy fuel engines, for the common rail system is mature and the injection pressure reaches 30 MPa or higher^[13-15]. But the mechanical system is too complicated to miniaturize, and difficult to apply to small aviation piston engines.

Currently, there are two miniaturized DI solutions for two-stroke engines, namely, air-assisted direct injection (AADI) and self-pressurized direct injection^[16], as shown in Fig.1. AADI uses compressed air to promote high-quality spray under a relatively low injection pressure^[17-18]. The atomization of the spray is not sensitive to the type of fuel and is especially suitable for high-viscosity and high-density heavy fuels^[19]. Thus, experimental and numerical studies have been carried out based on the AADI technique^[20-24]. However, the injection pressure is just 0.6 MPa, and the atomization is strongly affected by the ambient pressure, making it difficult to achieve a well-atomized stratified mixture^[25-26].

The self-pressurized injector is based on the water hammer effect in which the high-speed flowing liquid would generate large pressure due to the sudden drop in flow rate. The ram-tuned injection system developed by Küntschler et al. is the earliest self-pressurized injector^[27-28]. Heimberg improved the injector structure with the hydraulic impact method and designed the Ficht injection system^[29]. It had been applied on personal watercrafts, and test results showed that hydrocarbon (HC) and nitrogen oxide emissions had been reduced by 75%, and fuel consumption had been reduced by 30%^[30]. Strauss et al. of Bombardier updated the Ficht injection system to a new E-TEC injection system, and combined it with an optimized combustion chamber, resulting in an overall emissions reduction greater than 50%^[31-33]. Team from the University of Idaho designed a clean snowmobile for competition using a two-stroke engine equipped with E-TEC system, which had achieved significant improvements in high power, low emissions and long endurance^[34-36]. Winkler et al. found that the improvement of the

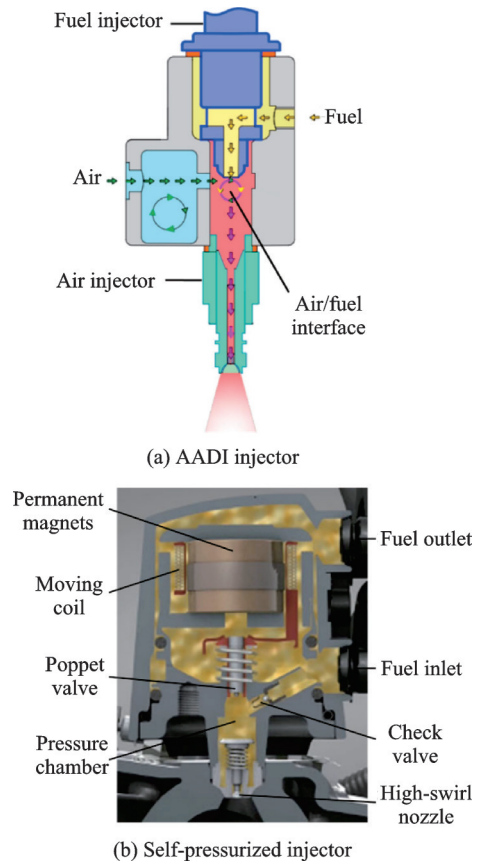


Fig.1 Schematic of two miniaturized DI solutions for two-stroke engines

power and emission performance level of E-TEC DI in part-load applications was unattainable by the low-pressure direct injection (LPDI) system, especially under idle and low loads^[37].

In addition to improving power, fuel consumption, and emissions, the self-pressurized injection system simplifies the fuel system and can be quickly applied on traditional port fuel injected engines. The high injection pressure allows stratified injection and multiple injection strategies to be used, where stratified injection strategy can further improve the fuel consumption and emissions under low engine load and speed^[38], and multiple injection strategy can maximize the charge cooling effect to suppress knock^[39].

1 Simulation Model for Spray

Before studying the application of self-pressurized injectors to engines, simulation research is required first, in which the first step is to study the spray model. The CFD software AVL Fire is em-

ployed to study the spray characteristics, and to further study the spray and combustion process in the cylinder.

In order to establish a complete spray model, the parameter acquisition of the injector and the selection of the spray sub-model are particularly important.

1.1 Basic parameters of self-pressurized injector

Before CFD simulation, it is necessary to provide parameters such as the fuel characteristics, the inner and outer diameters of the nozzle hole, the inner and outer cone angles of the spray, the fuel injection rate, and the injection pressure difference.

Part of the geometric parameters can be obtained by measuring the nozzle shaft needle. Fig. 2 (a) shows the needle at the nozzle exit under the microscope. The measured nozzle cross-sectional view is shown in Fig. 2(b).

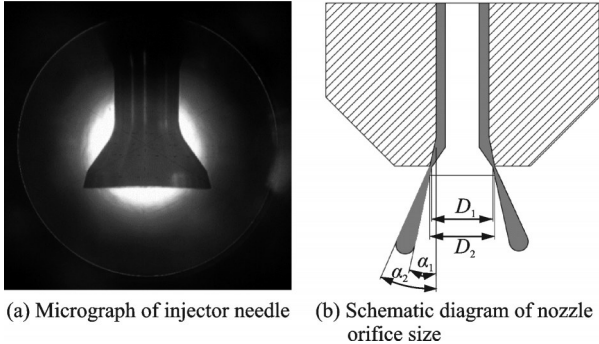


Fig. 2 Micrograph of injector needle and schematic diagram of nozzle orifice size

The fuel injection rate can be obtained by the flow characteristic test, and Fig. 3 shows the flow characteristic curve. The injection dead zone of the injector is 0.7 ms, and the slope of the line connecting the points where the fuel pulse width is greater than 0.7 ms is the fuel injection rate.

In order to facilitate the adjustment of fuel injection parameters in the simulation process of the whole machine, the following simplified assumptions are made for the fuel injection dynamic process of the self-boosting injector: the response process of the injector opening and closing phases is not considered; the injection pressure during the fuel injection

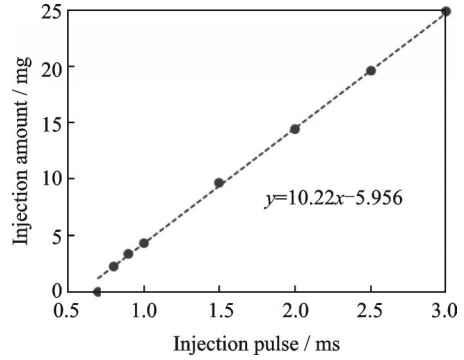


Fig. 3 Flow characteristic curve

Table 1 Injector parameters

Parameter	Value
Injection pressure /MPa	3.5
Fuel injection flow /($\text{g}\cdot\text{s}^{-1}$)	10.22
Nozzle inner diameter /mm	3.45
Needle cone angle /($^{\circ}$)	13.4
Needle lift / μm	100
Sheet velocity / ($\text{m}\cdot\text{s}^{-1}$)	≈ 90

process is not considered; the fuel injection rate is maintained at a fixed value.

1.2 Break-up model for self-pressurized injector

The CFD software AVL Fire provides a variety of break-up models. According to the characteristics of the outward-opening swirl nozzle and the hollow cone spray, two suitable break-up models are selected.

1.2.1 Han Sheet model

The sheet model represents a simple, semi-empirical primary break-up model used to determine the initial spray conditions such as the sheet thickness, velocity, and break-up length. The sheet thickness h of the liquid sheet at the nozzle orifice is computed as^[40]

$$h = \left[\frac{12A\dot{m}_1\mu_1}{\pi\rho_1 d_{\text{out}}\Delta p} \cdot \frac{(1+X)}{(1-X)^2} \right]^{0.5} \quad (1)$$

$$X = \frac{(d_{\text{out}} - 2h)^2}{d_{\text{out}}^2} \quad (2)$$

where \dot{m}_1 is liquid mass flow, μ_1 liquid dynamic viscosity, ρ_1 liquid density, Δp the pressure difference between liquid and gas, d_{out} outer orifice diameter of the nozzle, and X the ratio of air core to total area as Eq.(2).

Velocity coefficient k_v is defined as the ratio of the actual discharge velocity v to the theoretical velocity corresponding to the total pressure differential across the nozzle, as shown in Eq.(3).

$$k_v = \frac{v}{(2\Delta p/\rho_1)^{0.5}} \quad (3)$$

It has been shown that k_v can be related to nozzle dimensions and spray cone angle α_{out} by Eq.(4)^[41], where C_3 is a constant introduced by Lefebvre et al. to fit different injector designs, and the standard setting is 1.17 and should be modified according to the actual discharge velocity^[40].

$$k_v = \frac{C_3}{\cos\theta} \cdot \left(\frac{1-X}{1+X} \right)^{0.5} \quad (4)$$

The break-up length B_L of the liquid sheet is obtained from Clark and Dombrowski by Eq.(5)^[42].

$$B_L = B \cdot \left[\frac{\rho_l \cdot \sigma \cdot \ln(\eta/\eta_0) \cdot h \cdot \cos\theta}{\rho_g \cdot v_{rel}^2} \right]^{0.5} \quad (5)$$

where σ is gas-liquid surface tension, $\ln(\eta/\eta_0)$ experimentally defined parameter, ρ_g gas density, and v_{rel} the relative velocity between liquid and gas.

The Han Sheet model was originally developed for inwardly opening swirl nozzles. Studies showed that this model is also suitable for outward-opening swirl nozzles, but there are huge differences in parameter settings. The sheet thickness h of the outwardly-opening swirl nozzle is limited to the nozzle gap when the injector is fully opened. Regardless of the influence of cavitation, the relationship between the sheet thickness h and the needle lift H of the shaft needle and the cone angle α_1 at the outlet is

$$h = H \sin \alpha_1 \quad (6)$$

The relationship between the actual discharge velocity v of the sheet and the liquid mass flow \dot{m}_1 and the sheet thickness h is

$$v = \frac{\dot{m}_1/\rho_1}{\frac{\pi}{4} \left[d_{out}^2 - (d_{out} - 2h)^2 \right]} \quad (7)$$

Adjust the parameters in the software AVL Fire to make the simulated values of the sheet thickness and velocity consistent with the calculated values, thereby completing the setting of the break-up model.

In summary, the Han Sheet model can be used

for outward-opening swirl nozzles, but the parameter settings are quite different. When the fuel type, fuel injection flow rate, or injection pressure difference change, the sheet thickness calculated by the simulation will also change, but the real sheet thickness is basically unchanged. Therefore, the parameters need to be re-adjusted every time, making the application of the Han Sheet model more complicated.

1.2.2 KH-RT model

In this model Kelvin-Helmholtz (KH) surface waves and Rayleigh-Taylor (RT) disturbances should be in continuous competition of breaking up the droplets^[42-43]. The KH mechanism is favored by high relative velocities and high ambient density. The RT mechanism is driven by rapid deceleration of the droplets causing the growth of surface waves at the droplet stagnation point. The WAVE model equations^[44] are as follows

$$R_a = C_1 \Lambda \quad (8)$$

$$t_a = \frac{3.7C_2 R}{\Lambda \Omega} \quad (9)$$

$$\Lambda = f(We_c, Oh_d) \quad (10)$$

$$\Omega = f(We_c, Oh_d) \quad (11)$$

where R is parent drop diameter, R_a child drop diameter, t_a the break-up time, Λ wavelength, Ω wave growth rate, We_c continuous phase property and Oh_d droplet property.

The RT disturbances are described by the fastest growing frequency Ω and the corresponding wave number K .

$$\Omega_i = \sqrt{\frac{2}{3\sqrt{3\sigma}} \cdot \frac{g_i |\rho_d - \rho_c|^{1.5}}{\rho_d + \rho_c}} \quad \tau_i = C_5 \frac{1}{\Omega_i} \quad (12)$$

$$k_i = \sqrt{\frac{g_i |\rho_d - \rho_c|}{3\sigma}} \quad \Lambda_i = C_4 \frac{\pi}{K_i} \quad (13)$$

Here g is the deceleration in the direction of travel. If the wave length Λ is small enough to be growing on the droplet's surface and the characteristic RT break-up time τ has passed, the droplets will be atomized and their new sizes are assumed to be proportional to the RT wave length. The break-up length L is calculated as

$$L = C_3 \sqrt{\frac{\rho_d}{\rho_c}} d_o \quad (14)$$

Droplets within the break-up length L are considered to undergo only KH break-up, whereas further downstream both mechanisms are present. The normal velocity component given to the child parcels is calculated from disturbance wavelength and growth rate modified by model parameter C_8 .

$$V_{\text{norm}} = C_8 \cdot \Lambda \cdot \Omega \quad (15)$$

The KH-RT model is suitable for break-up with high relative velocity or rapid deceleration of droplets, while the hollow cone spray has a high velocity at the nozzle outlet, and has a large deceleration after sheet break-up. But the KH-RT model cannot be directly applied to the hollow cone spray, so some adjustments are needed.

Suppose that the outwardly-opening swirl nozzle is replaced with a large number of orifice nozzles in the circumferential direction. The cylindrical sprays emitted by each orifice nozzle are connected to each other to form a hollow cone-shaped liquid sheet with uneven thickness. Under this equivalent condition, the KH-RT model can be used, and the initial droplet diameter D_0 of each sub orifice nozzle can be calculated according to the method of equal spray cross-sectional area as follows.

$$\frac{\pi}{4} [d_{\text{out}}^2 - (d_{\text{out}} - 2h)^2] = \frac{\pi}{4} D_0^2 \frac{\pi(d_{\text{out}} - h)}{D_0} \quad (16)$$

In summary, the adjusted KH-RT model is suitable for the spray with an outward-opening swirl nozzle. The initial droplet size is derived from the spray cross-sectional area of the nozzle orifice, and there is no need to modify the nozzle-related parameters during the simulation, which makes the application of the KH-RT model convenient.

2 Spray Simulation Model Verification

In order to ensure the accuracy of the spray model, it is necessary to carry out the comparison and correction in conjunction with the spray test.

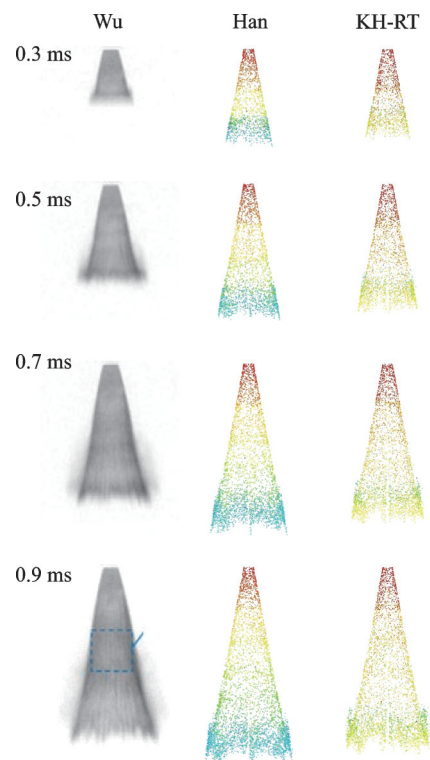
2.1 Variable pressure in constant volume bomb

Constant volume bomb test is a common method to obtain spray characteristics under different environmental pressures. Trejo et al.^[45] and Wu et al.^[16] have carried out constant volume bomb tests on self-pressurized fuel injectors. Among them, the spray test images obtained by Wu et al. are clearer and serve as a reference for spray simulation in this article.

The initial and boundary conditions of the simulation are shown in Table 2. The simulation results of two spray models and the comparison with the experiment are shown in Fig.4 and Fig.5, in which the sizes of all pictures have been adjusted to 50 mm in width and 100 mm in the maximum height.

Table 2 Constant volume bomb simulation parameters

Parameter	Value
Fuel type	Isooctane(C ₈ H ₁₈)
Ambient gas	Air
Ambient pressure/MPa	0.1/0.4
Ambient temperature/°C	25
Fuel temperature/°C	40
Injection pulse/ms	2.0



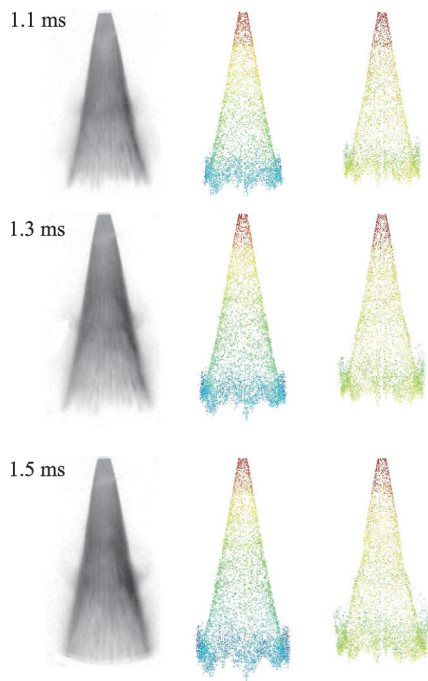


Fig.4 Comparison of spray patterns at pressure of 0.1 MPa

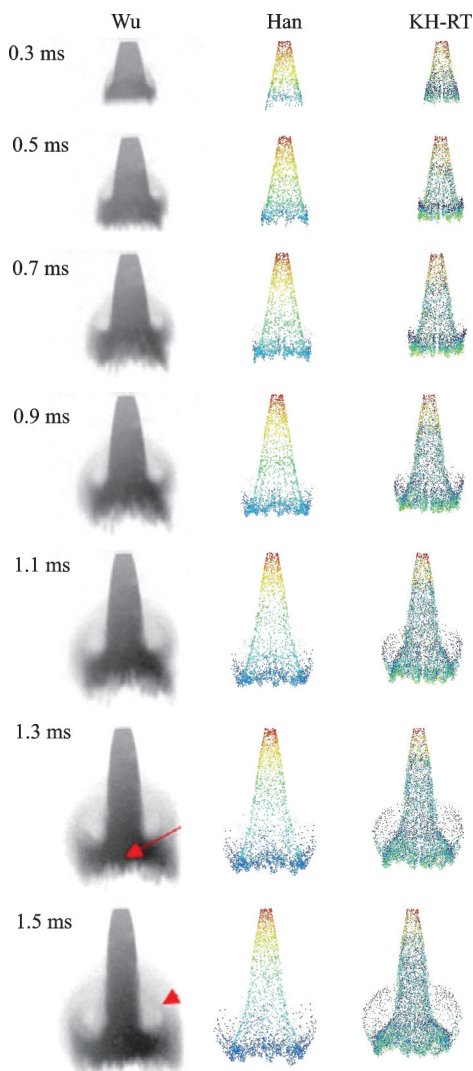


Fig.5 Comparison of spray patterns at pressure of 0.4 MPa

There are some points to explain before analyzing and comparing. The width of the spray tip is different in the spray images of simulation and experiment, in which the size of the simulation is consistent with the actual nozzle size, while nozzle occlusion affects the extraction of the spray tip in the experiment image. The other is that the test spray exceeds the boundary of the window at 1.5 ms with an ambient pressure of 0.1 MPa, making the end of the spray into a circular arc shape.

In the simulation results, when the ambient pressure is 0.1 MPa, the spray patterns obtained by the simulation of the two models are basically consistent with the experimental. Because the process of injector opening and the establishment of the spray flow is ignored, the penetration of simulation in the initial stage is larger than the experiment. The Han Sheet model ignores the effect of the liquid sheet with air before it breaks, so the penetration distance is larger than the result of KH-RT model. When the ambient pressure is 0.4 MPa, both models can simulate the coalescence of the far-field spray after breaking up to form a recirculating vortex, and the KH-RT model can better simulate the shrinking trend of the spray cone angle no matter in the near field or the far field.

In summary, in the spray simulation of variable ambient pressure in the constant volume bomb, the spray pattern simulated by the KH-RT model is closer to the spray pattern referenced in the experiment.

2.2 Variable flow velocity in a wind tube

Strauss et al. found that engines with different in-cylinder air flows can exhibit significantly different behaviors with similar fuel sprays, and built a test fixture as shown in Fig.6, to evaluate fuel sprays into air counter flows^[33].

The initial and boundary conditions of the simulation are shown in Table 3. The simulation results of the two spray models and the comparison with the experiment are shown in Fig.7. Since the spray tip is blocked by the injector bracket, the length is estimated to be 14 mm according to the nozzle size

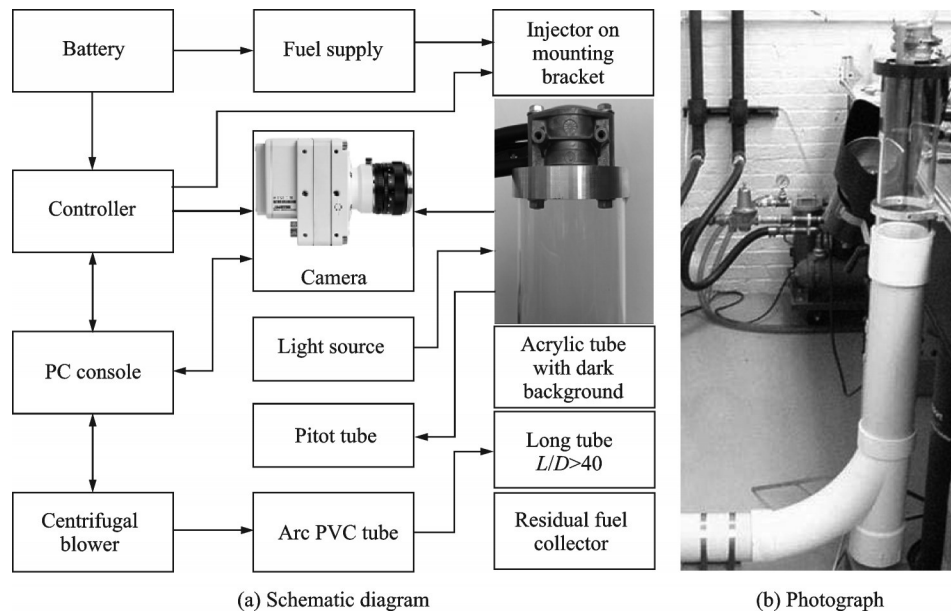


Fig.6 Experimental setup for wind tube

Table 3 Wind tube simulation parameters

Parameter	Value
Fuel type	Isooctane(C ₈ H ₁₈)
Ambient gas	Air
Air velocity/(m·s ⁻¹)	0/10/20/30/40
Ambient temperature/°C	25
Fuel temperature/°C	25
Injection pulse/ms	2.0

and spray cone angle. Therefore, the simulation result output image size is adjusted to 75 mm ×

71 mm, where the test image size is 75 mm × 56 mm. The images of 1 ms and 2 ms after the penetration reaches 14 mm are selected for comparison.

With the air velocity of 0 m/s, the spray is basically the same as the constant volume bomb test at 1ms, but there is a clear boundary between near-field and far-field spray at 2 ms. This is because in the late stage of injection, the injection pressure drops until

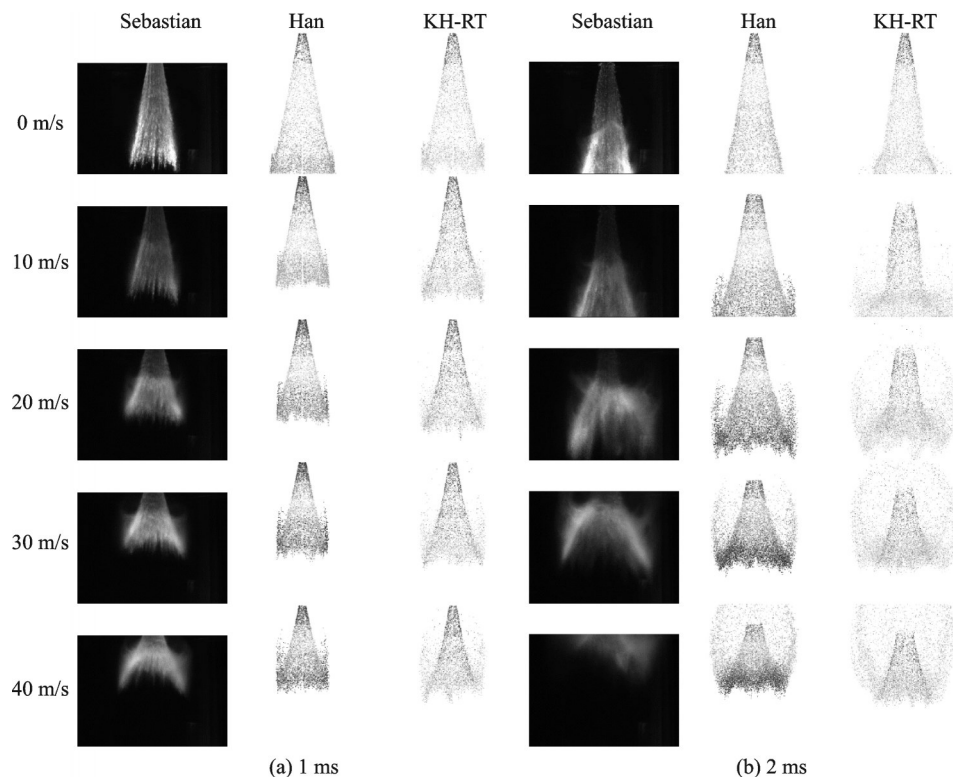


Fig.7 Comparison of spray patterns at variable flow velocities

the nozzle is closed, which causes the fuel injection rate to drop and the spray cone angle to decrease. However, the simulation process ignores the pressure and flow changes at the end of the injection, so the simulation image does not show this phenomenon. Therefore, the comparison between the simulation and the test is mainly based on the time of 1 ms.

With the increase of the air velocity, the spray cone angle of the near-field spray gradually increases under the force of the airflow. The cone angle of the far-field spray increases more obviously, and a vortex ring is formed after the liquid sheet is broken. In the simulation image, the KH-RT model simulates the change of the spray cone angle better, and therefore the axial penetration is closer to the test. For the spray penetration, the results of the KH-RT model are closer at low velocity, while the Han Sheet model is closer at the high velocity.

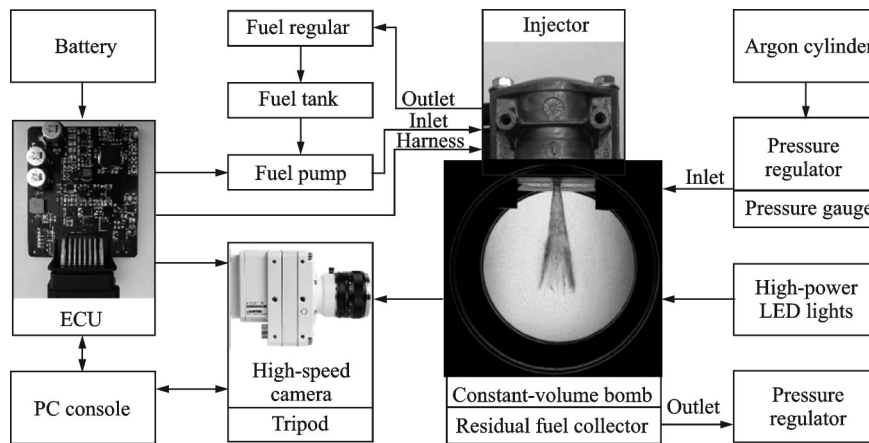
In summary, under the force of the air stream, the spray liquid sheet transitions from a conical shape to a trumpet shape before breaking, and the droplets formed by the breaking of the liquid sheet are more uniform, resulting in a sharp drop in the penetration. The

Han Sheet model fails to simulate the deformation process of the liquid sheet well, while the KH-RT model performs better. The spray model still needs to be corrected by the dynamic data of pressure and flow during the injection process.

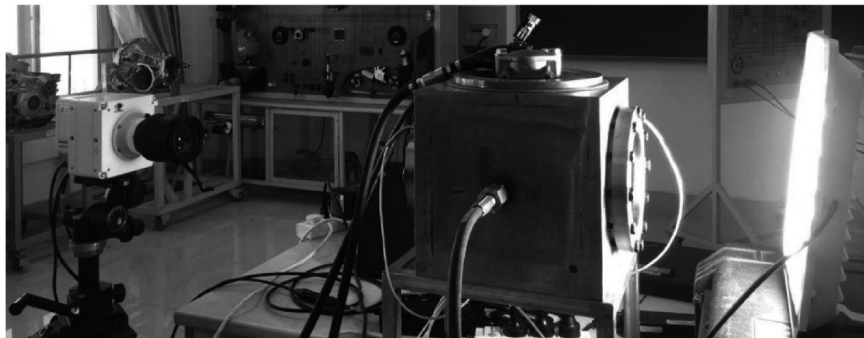
3 Aviation Kerosene Spray Test

Self-pressurized fuel injector is a miniaturized direct injection solution, which is very suitable for light and high-power aviation piston heavy fuel engines. The spray tests in the current literatures all use isoctane standard fuel. Therefore it is of innovative value to study the aviation kerosene spray characteristics of self-pressurized injector.

The experimental setup is shown in Fig.8. The self-pressurized injector is installed on the constant volume bomb and is driven by the self-developed electronic control unit (ECU) together with the fuel pump, and the ECU is controlled by the self-developed interface software on the PC console. The constant-volume bomb is filled with argon supplied by an argon cylinder, and pressure regulators at the in-



(a) Schematic diagram



(b) Photograph

Fig.8 Experimental setup

let and outlet control the pressure. The high-speed camera, model Phantom VEO410L, is controlled by the PC through PCC software. When the self-developed ECU drives the injector, another synchronous signal is transmitted to the high-speed camera via the BNC cable.

The initial and boundary conditions of the test are shown in Table 4.

The experiment results are shown in Fig.9, in which the sizes of all pictures have been adjusted to 50 mm in width. In order to accurately capture the spray at the nozzle mouth, set the main optical axis of the high-speed camera to be concentric with two

Table 4 Aviation kerosene test parameters

Parameter	Value
Fuel type	RP-3
Ambient gas	Argon
Ambient pressure/MPa	0.1/0.2/0.4
Ambient temperature/°C	25
Fuel temperature/°C	25
Injection pulse/ms	2.0

pieces of quartz glass. Therefore, when extracting the spray from the background image, the gray scale of the spray near the nozzle is low due to the influence of the bottom surface of the injector bracket, but this does not affect the obtained spray pattern.

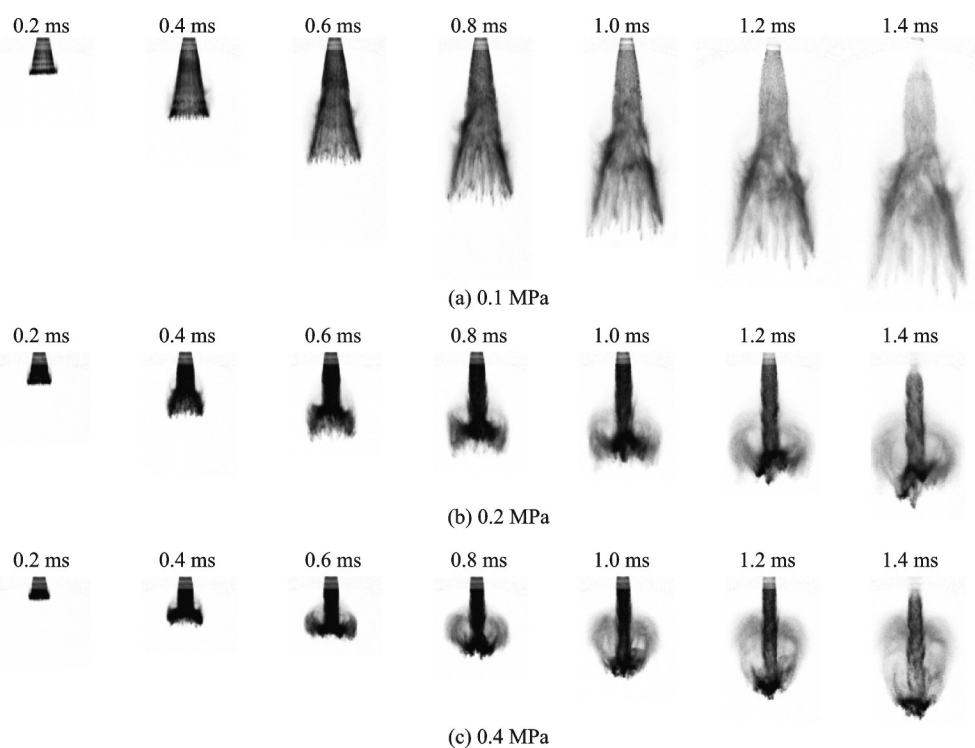


Fig.9 Aviation kerosene spray at variable pressures

When the ambient pressure is 0.1 MPa, the near-field spray is conical. At 0.6 ms, the boundary of far and near field sprays can be clearly observed, where the liquid sheet is broken and discrete jet string and detached droplets formed. After 1 ms, the gray scale of the near-field spray drops significantly, because the fuel flow rate drops due to the decrease in the injection pressure at the late stage of the injection. The spray pattern of kerosene fuel is significantly different from that of iso-octane fuel.

When the ambient pressure increases, the penetration at the early stage of the spray basically decreases proportionally. The spray is difficult to maintain a conical shape and it quickly transitions to a cylindrical shape, and even shrinks further before breaking. The position where sheet break is no longer fixed, which gradually moves downward as the spray develops, and the spray breaking position is basically the same under the pressures of 0.2 MPa and 0.4 MPa. After the spray is broken, there are

no more discrete jet strings but only droplets. The shape of the vortex ring formed by the droplets is also different, which is closer to a circle at an ambient pressure of 0.2 MPa, and closer to a heart shape at 0.4 MPa. The greater ambient pressure, the faster the droplet kinetic energy decreases, which leads to the drop of spray penetration and the change of the vortex ring shape.

In general, the difference in physical and chemical properties of aviation kerosene and isooctane leads to obvious differences in sprays. The spray of aviation kerosene has a smaller cone angle, larger penetration and faster breaking, easier to produce vortex ring.

4 Conclusions

This paper reviews the recent development of the UAV power unit and the application of direct injection technology, with an emphasis on two miniaturized direct injection technologies: AADI and self-pressurized injection. The AADI technology has been proved to provide excellent spray characteristics with particle size about 7 μm . The self-pressurized injection technology can provide an injection pressure of 5 MPa, and there is still considerable room for improvement. This paper has carried out simulation and experimental research on self-pressurized injectors, and the conclusions obtained are as follows.

(1) There are two break-up models in the AVL Fire software suitable for the hollow cone spray of self-pressurized fuel injector. When applying the Han Sheet model, the thickness of the liquid sheet needs to be adjusted according to the gap of the open nozzle, which makes the parameter setting inconvenient. When applying the KH-RT model, an equivalent assumption needs to be made, and the application of the model is convenient.

(2) The spray simulated by the Han Sheet model and KH-RT model can basically simulate the spray development process under the two pressures of the constant volume bomb environment, and the KH-RT model fits the spray cone angle better. The process of fuel pressure establishment and nozzle

opening has a significant effect on the initial penetration distance of the spray, which affects the accuracy of the initial spray simulation.

(3) The air counter flow has a huge impact on the hollow cone spray morphology, especially the liquid sheet part before spray break-up. The Han Sheet model fails to simulate this phenomenon, resulting in a smaller axial penetration. The process of fuel pressure drop and nozzle closing has a significant effect on the initial spray velocity and broken length, which affects the accuracy of the final spray simulation.

(4) The aviation kerosene spray test shows that the different physical and chemical properties of kerosene and gasoline lead to differences in spray patterns. This difference is more pronounced on swirl nozzle than on traditional orifice nozzle. Under normal pressure conditions, it is already difficult for kerosene spray to maintain the initial spray cone angle. When the background pressure increases by 0.1 MPa, the kerosene spray becomes cylindrical, which has a serious negative impact on the atomization process and particle size of the spray.

References

- [1] AUSTIN R. Unmanned aircraft systems: UAVS design, development and deployment[M]. [S.l.]: John Wiley & Sons, 2011.
- [2] BOUKOBERINE M N, ZHOU Z, BENBOUZID M. A critical review on unmanned aerial vehicles power supply and energy management: Solutions, strategies, and prospects[J]. Applied Energy, 2019, 255: 113823.
- [3] BONGERMINO E, MASTROROCOCO F, TOMASELLI M, et al. Model and energy management system for a parallel hybrid electric unmanned aerial vehicle[C]//Proceedings of 2017 IEEE 26th International Symposium on Industrial Electronics (ISIE). [S.l.]: IEEE, 2017: 1868-1873.
- [4] SCAPPIN F, STEFANSSON S H, HAGLIND F, et al. Validation of a zero-dimensional model for prediction of NO_x and engine performance for electronically controlled marine two-stroke diesel engines[J]. Applied Thermal Engineering, 2012, 37: 344-352.
- [5] HEYWOOD J B, SHER E. The two-stroke cycle engine: Its development, operation and design[M]. [S.l.]: Routledge, 2017.

- [6] KRISHNA A S, MALLIKARJUNA J M, KUMAR D. Effect of engine parameters on in-cylinder flows in a two-stroke gasoline direct injection engine[J]. *Applied Energy*, 2016, 176: 282-294.
- [7] SHER E. Scavenging the two-stroke engine[J]. *Progress in Energy and Combustion Science*, 1990, 16(2): 95-124.
- [8] Department of Defense. Unmanned aerial vehicles roadmap 2002—2027[R]. Washington, USA:[s.n.], 2002.
- [9] CHEN L, LIANG Z, LIU H, et al. Sensitivity analysis of fuel types and operational parameters on the particulate matter emissions from an aviation piston engine burning heavy fuels[J]. *Fuel*, 2017, 202: 520-528.
- [10] DUDDY B J, LEE J, WALLUK M, et al. Conversion of a spark-ignited aircraft engine to JP-8 heavy fuel for use in unmanned aerial vehicles[J]. *SAE International Journal of Engines*, 2011, 4(1): 82-93.
- [11] LIU R, WEI M, YANG H Q. Cold start control strategy for a two-stroke spark ignition diesel-fuelled engine with air-assisted direct injection[J]. *Applied Thermal Engineering*, 2016, 108: 414-426.
- [12] NORA D M, LANZANOVA T D M, ZHAO H. Effects of valve timing, valve lift and exhaust backpressure on performance and gas exchanging of a two-stroke GDI engine with overhead valves[J]. *Energy Conversion and Management*, 2016, 123: 71-83.
- [13] NING L, DUAN Q, WEI Y, et al. Effects of injection timing and compression ratio on the combustion performance and emissions of a two-stroke DISI engine fuelled with aviation kerosene[J]. *Applied Thermal Engineering*, 2019, 161: 114124.
- [14] MONTANARO U, GAETA D A, GIGLIO V. Adaptive tracking control of a common rail injection system for gasoline engines: A discrete-time integral minimal control synthesis approach[J]. *IEEE Transactions on Control Systems Technology*, 2012, 21(5): 1940-1948.
- [15] CHEN H, GONG X, LIU Q, et al. Triple-step method to design non-linear controller for rail pressure of gasoline direct injection engines[J]. *IET Control Theory & Applications*, 2014, 8(11): 948-959.
- [16] WU H, ZHANG F, ZHANG Z, et al. Experimental investigation on the spray characteristics of a self-pressurized hollow cone injector[J]. *Fuel*, 2020, 272: 117710.
- [17] CATHCART G, ZAVIER C. Fundamental characteristics of an air-assisted direct injection combustion system as applied to 4-stroke automotive gasoline engines: SAE Technical Paper, No. 2000-01-0256[R]. [S.l.]: SAE, 2000.
- [18] CATHCART G, DICKSON G, AHERN S. The application of air-assist direct injection for spark-ignited heavy fuel 2-stroke and 4-stroke engines: SAE Technical Paper, No. 2005-32-0065[R]. [S.l.]: SAE, 2005.
- [19] HU J, LIU B, ZHANG C, et al. Experimental study on the spray characteristics of an air-assisted fuel injection system using kerosene and gasoline[J]. *Fuel*, 2019, 235: 782-794.
- [20] BORETTI A, JIN S H, BREAR M, et al. Experimental and numerical study of a spark ignition engine with air-assisted direct injection[J]. *Proceedings of the Institution of Mechanical Engineers, Part D: Journal of Automobile Engineering*, 2008, 222(6): 1103-1119.
- [21] JIN S H, BREAR M, WATSON H, et al. An experimental study of the spray from an air-assisted direct fuel injector[J]. *Proceedings of the Institution of Mechanical Engineers, Part D: Journal of Automobile Engineering*, 2008, 222(10): 1883-1894.
- [22] PADALA S, BANSAL A, RAMESH A. Studies on an air assisted gasoline direct injection system for a two-stroke engine: SAE Technical Paper, No. 2008-28-0048[R]. [S.l.]: SAE, 2008.
- [23] WU H, WANG L, WU Y, et al. Spray performance of air-assisted kerosene injection in a constant volume chamber under various in-cylinder GDI engine conditions[J]. *Applied Thermal Engineering*, 2019, 150: 762-769.
- [24] YANG B, DUAN Q, LIU B, et al. Parametric investigation of low-pressure dual-fuel direct injection on the combustion performance and emissions characteristics in a RCCI engine fueled with diesel and CH₄[J]. *Fuel*, 2020, 260: 116408.
- [25] GAO H, ZHANG F, ZHANG Z, et al. Experimental investigation on the spray characteristic of air-assisted hollow-cone gasoline injector[J]. *Applied Thermal Engineering*, 2019, 151: 354-363.
- [26] GAO H, ZHANG F, ZHANG Z, et al. Trajectory deviation of target jet of air-assisted spray under different conditions[J]. *Fuel*, 2019, 249: 252-263.
- [27] KÜNTSCHER V, STAN C. A new Diesel mixture formation approach for small high-speed two-stroke en-

- gine applications[C]//Proceedings of SAE International Congress and Exposition. Detroit, USA:SAE, 1989.
- [28] STAN C. Experimental analysis of the fuel spray characteristics for DI high speed engines using a ram tuned injection system[J]. SAE Transactions, 1997: 2178-2189.
- [29] HEIMBERG W. Ficht pressure surge injection system: SAE Technical Paper, No.93A079[R].[S.l.]: SAE, 1993.
- [30] FUKAMI Y, WATABE S, JINJA Y, et al. Superiority of newly developed direct-injection engine over conventional engine for personal watercraft: SAE Technical Paper, No.2001-01-1787[R].[S.l.]: SAE, 2001.
- [31] STRAUSS S, ZENG Y, MONTGOMERY D T. Optimization of the E-TEC™ combustion system for direct-injected two-stroke engines toward 3-star emissions[C]//Proceedings of Small Engine Technology Conference & Exposition. Madison, USA: [s. n.] , 2003.
- [32] ZENG Y, STRAUSS S. Modeling of scavenging and plugging in a twin-cylinder two stroke engine using CFD: SAE Technical Paper, No.2003-32-0020[R].[S.l.]: SAE, 2003.
- [33] STRAUSS S, ZENG Y. The effect of fuel spray momentum on performance and emissions of direct-injected two-stroke engines[C]//Proceedings of 2004 Small Engine Technology Conference. Graz, Austria: [s.n.],2004.
- [34] BRADBURY N, SCHIERMEIER R, HARRIS T, et al. University of Idaho's clean snowmobile design using a direct-injection two-stroke: SAE Technical Paper, No.2005-01-3680[R].[S.l.]: SAE, 2005.
- [35] BRADBURY N, FINDLAY A, JOHNSON J, et al. University of Idaho's clean snowmobile design using a direct-injection two-stroke: SAE Technical Paper, No. 2006-32-0050[R].[S.l.]: SAE, 2006.
- [36] HARKER N, DENBRAVEN K R, JOHNSON J, et al. University of Idaho's clean snowmobile design using a direct-injection two-stroke engine: SAE Technical Paper, No. 2008-32-0031[R].[S.l.]: SAE, 2008.
- [37] WINKLER F, OSWALD R, SCHOEGL O, et al. Characterization of different injection technologies for high performance two-stroke engines: SAE Technical Paper, No.2016-32-0001[R].[S.l.]: SAE, 2016.
- [38] JOHNSON J, BRAVEN D K R. Comparison of homogeneous, stratified and high-squish stratified combustion in a direct-injected two-stroke engine: SAE Technical Paper, No.2008-32-0030[R].[S.l.]: SAE, 2008.
- [39] HAN T, SINGH R, LAVOIE G, et al. Multiple injection for improving knock, gaseous and particulate matter emissions in direct injection SI engines[J]. Applied Energy, 2020, 262: 114578.
- [40] LEFEBVRE A H, MCDONELL V G. Atomization and sprays[M]. [S.l.]: CRC Press, 2017.
- [41] HAN Z, FAN L, REITZ R D. Multidimensional modeling of spray atomization and air-fuel mixing in a direct-injection spark-ignition engine[C]//Proceedings of International Congress & Exposition.[S.l.]: [s. n.],1997.
- [42] CLARK C J, DOMBROWSKI N. Aerodynamic instability and disintegration of inviscid liquid sheets[J]. Proceedings of the Royal Society of London. A. Mathematical and Physical Sciences, 1972, 329 (1579) : 467-478.
- [43] KÜNSBERG-SARRE C, TATSCHL R. Spray modeling/atomisation—Current status of break-up models[C]//Proceedings of IMECHE-Seminar.[S.l.]: [s. n.], 1998: 15-16.
- [44] REITZ R D, BRACCO F V. Mechanism of atomization of a liquid jet[J]. The Physics of Fluids, 1982, 25 (10): 1730-1742.
- [45] TREJO J R I C. Direct injection system for a two-stroke engine[D]. Gothenburg: Chalmers University of Technology, 2011.

Acknowledgements This work was supported by the National Natural Science Foundation of China (No.51865031), the State Key Laboratory of Engines of Tianjin University (No.K2020-05), and the Natural Science Foundation of the Jiangsu Higher Education Institutions of China (No. 20KJB470014).

Authors Dr. JI Haocheng received the B.S. and Ph.D. degrees in vehicle engineering and power engineering from Nanjing University of Aeronautics and Astronautics in 2012 and 2020, respectively. He is currently affiliated with the School of Mechanical and Power Engineering, Nanjing Tech University. His current research interests include electronic control technology for two-stroke engines.

Dr. LIU Rui received the B.S. and Ph.D. degrees in vehicle engineering from Nanjing University of Aeronautics and Astronautics in 2011 and 2017, respectively. He is currently af-

filiated with School of Mechanical and Power Engineering, Nanjing Tech University. His current research interests include the control and numerical simulation of direct injection internal combustion engines.

Author contributions Dr. JI Haocheng designed the study, compiled the models, conducted the analysis, interpreted the results and wrote the manuscript. Dr. LIU

Rui designed the spray experiment and contributed data for the analysis. Dr. LI Jing contributed to the discussion and background of the study. Dr. ZHAI Buyun contributed to the spray experiment. All authors commented on the manuscript draft and approved the submission.

Competing interests The authors declare no competing interests.

(Production Editor: WANG Jing)

自增压式喷油器的燃油喷雾特性仿真及试验研究

季昊成¹, 刘锐¹, 李晶¹, 翟步云²

(1. 南京工业大学机械与动力工程学院, 南京 211816, 中国; 2. 金城集团有限公司小型动力项目部, 南京 210002, 中国)

摘要: 自增压式喷油器作为一种小型化的直接喷射方案, 对于以点燃式二冲程重油发动机为典型的小型航空活塞发动机具有重要意义。直喷喷油器的喷雾特性是一个重要的应用先决条件。本文采用计算流体动力学软件 AVL Fire 对其喷雾特性进行研究。在 Han Sheet 和 KH-RT 两种破碎模型的基础上分别建立了两种喷雾模型, 并根据文献中的两种喷雾试验条件进行了模拟工作。对比结果表明, 在定容弹试验中, 两组环境压力下模拟得到的喷雾形态与试验相近, 其中采用 KH-RT 模型模拟的喷雾可以更好地拟合喷雾在近场收缩现象以及远场的涡环现象。在管道试验中, 5 组流场流速下模拟得到的喷雾形态与试验相近, 其中采用 KH-RT 模型模拟的喷雾可以更好地拟合喷雾的扩张现象以及远场的涡环现象。本文还试验研究了自增压式喷油器应用 RP-3 航空煤油的喷雾特性。试验结果表明, 由于煤油粘度较高, 中空锥形喷雾易收缩, 导致喷雾锥角减小, 贯穿距离增大。因而, 环境压力的变化对煤油喷雾形态的影响更大。

关键词: 直接喷射; 喷雾特性; 活塞发动机; 自增压式喷油器